

Studies on the electroproduction of ϕ meson

Sang-Ho Kim^{1,*} and Seung-il Nam^{1,2,†}

¹*Department of Physics, Pukyong National University (PKNU), Busan 48513, Republic of Korea*

²*Asia Pacific Center for Theoretical Physics (APCTP), Pohang 37673, Republic of Korea*

(Dated: April 26, 2022)

We investigate ϕ -meson electroproduction off the proton target, i.e., $\gamma^* p \rightarrow \phi p$, by employing a tree-level effective Lagrangian approach in the kinematical ranges of $Q^2 = (0-4)$ GeV², $W = (2-5)$ GeV, and $|t| \leq 2$ GeV². In addition to the universally accepted Pomeron exchange, we consider various meson exchanges in the t channel with the Regge method. Direct ϕ -meson radiations in the s - and u -channels are also taken into account. We find that the Q^2 dependence of the transverse (σ_T) and longitudinal (σ_L) cross sections are governed by Pomeron and a_0 scalar meson exchanges, respectively. Meanwhile, the contributions of (π, η) pseudoscalar- and $f_1(1285)$ axial-vector-meson exchanges are much more suppressed. The results of the interference cross sections (σ_{LT}, σ_{LT}) and the spin-density matrix elements indicate that s -channel helicity conservation (SCHC) holds at $Q^2 = (1-4)$ GeV². The result of the parity asymmetry yield $P \simeq 0.95$ at $W = 2.5$ GeV, meaning that natural-parity exchange dominates the reaction process. Our numerical results are in fair agreement with the experimental data and thus the use of our effective Reggeized model is justified over the considered kinematical ranges of Q^2 , W , and t .

PACS numbers: 13.60.Le, 13.40.-f, 14.20.Jn, 14.20.Gk

Keywords: ϕ -meson electroproduction, Pomeron, a_0 scalar meson, effective Lagrangian approach, Regge method.

* E-mail: shkim@pknu.ac.kr

† E-mail: sinam@pknu.ac.kr

I. INTRODUCTION

Exclusive electroproduction of vector mesons is a suitable place to test model predictions in a kinematic region where the transition between the hadronic and partonic domains is involved according to the ranges of the photon virtuality Q^2 and the photon center-of-mass (c.m.) energies W . The ZEUS and H1 Collaborations at HERA accumulated a lot of data for electroproductions of ρ - [1, 2], ω - [3], and ϕ - [2, 4, 5] light vector-mesons over wide ranges of Q^2 and W (e.g., $2.5 \leq Q^2 \leq 60 \text{ GeV}^2$ and $35 \leq W \leq 180 \text{ GeV}$ at H1 [2]). The scale is large enough for perturbative Quantum Chromodynamics (pQCD) to be employed. Meanwhile, the Cornell group at the Laboratory of Nuclear Studies (LNS) at Cornell University [6–8], the CLAS Collaboration at Jefferson Lab [9–13], and the HERMES Collaboration at DESY [14–17] performed the experiments of vector-meson electroproductions at relatively low Q^2 and W values (e.g., $1.0 \leq Q^2 \leq 7.0 \text{ GeV}^2$ and $3.0 \leq W \leq 6.3 \text{ GeV}$ at HERMES). Then we get access to the soft scale and pose a question. What ranges in Q^2 and W are more adequate for the hadronic or partonic descriptions?

A series of works on electro- and photoproductions of light vector-mesons was carried out by Laget *et al.* previously based on the Regge phenomenology [18–21]. The exchanges of meson Regge trajectories and of a Pomeron trajectory are considered in the t channel with phenomenological form factors for each vertex. The Q^2 and t dependences on the cross sections at low photon energies ($W \sim \text{a few GeV}$) are reasonably described. Then Ref. [22] developed the work for ρ -meson electroproduction by employing an effective Lagrangian approach with the updated CLAS data [9, 10]. The transverse and longitudinal parts of the cross sections are examined in some detail. The separated components help us to pin down the role of different meson exchanges and Pomeron exchange as well, which is difficult only with the study of the unpolarized total cross section.

In this paper, we take a similar approach for ϕ -meson electroproduction and test whether our hadronic description is applicable or not in the kinematical ranges of $Q^2 = (0\text{--}4) \text{ GeV}^2$, $W = (2\text{--}5) \text{ GeV}$, and $|t| \leq 2 \text{ GeV}^2$. We examine the Q^2 and t dependences on the transverse, longitudinal, and interference parts of the cross sections. The latter enables us to test s -channel helicity conservation (SCHC). The spin-density matrix elements of the produced ρ -meson are also analyzed in the helicity frame which is in favor of SCHC. Parity asymmetry is calculated to check the relative strengths of natural to unnatural parity exchanges in the t channel.

For this purpose, we utilize our recent results for ϕ -meson photoproduction, $\gamma p \rightarrow \phi p$ [23], where the relative contributions among the Pomeron and various meson exchanges were discussed in detail by analyzing a vast amount of CLAS data [24, 25]. The basic formalism used in Ref. [23] applied to the present work. However, the s -channel nucleon resonance contribution is excluded for brevity, although our kinematical range covers some high-mass resonance regions. Indeed, in ϕ -meson photoproduction, the N^* contribution is found to be crucial only for the backward ϕ -meson scattering angles with small magnitudes and does not change much the integrated cross sections [23], whereas the data for electro- and photoproductions of ρ - [22, 26] and ω - [12, 27] vector-mesons imply the necessity for the s -channel N^* contribution. We find that our hadronic approach provides a very successful description of the available experimental data over the considered kinematical ranges of Q^2 , W , and t .

The remaining part of this paper is organized as follows. In Sec. II, we define the kinematics of ϕ -meson electroproduction process. In Sec. III, we explain the general formalism of the effective Lagrangian approach. We present and discuss the numerical results in Sec. IV. The final section is devoted to the summary.

II. KINEMATICS

Let us first specify kinematics of the ϕ -electroproduction process $ep \rightarrow e\phi p$ drawn in Fig. 1 graphically. The four-momenta of the involved particles described in the hadron production plane are given by

$$\gamma^*(k_1) + p(p_1) \rightarrow \phi(k_2) + p(p_2), \quad (1)$$

in parentheses, where

$$\begin{aligned} k_1 &= (\sqrt{k^2 - Q^2}, 0, 0, k), & k_2 &= (\sqrt{p^2 + M_\phi^2}, p \sin \theta_\phi, 0, p \cos \theta_\phi), \\ p_1 &= (\sqrt{k^2 + M_N^2}, 0, 0, -k), & p_2 &= (\sqrt{p^2 + M_N^2}, -p \sin \theta_\phi, 0, -p \cos \theta_\phi). \end{aligned} \quad (2)$$

They are defined in the γ^*p center-of-mass (c.m.) frame where the z axis is set to be parallel to the direction of the virtual photon and the y axis normal to the hadron production plane along $\vec{k}_1 \times \vec{k}_2$. Here, the magnitudes of the three-momenta of the initial- and final-particles are given by

$$\begin{aligned} k &= \lambda(-Q^2, M_N^2, W^2)^{\frac{1}{2}} / (2W) = M_N \sqrt{\nu^2 + Q^2} / W, \\ p &= \lambda(M_\phi^2, M_N^2, W^2)^{\frac{1}{2}} / (2W), \end{aligned} \quad (3)$$

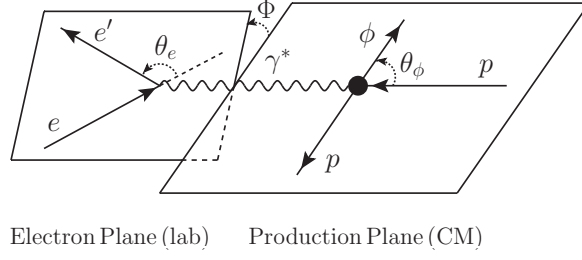


FIG. 1. Graphical representation of the electron scattering ($ee'\gamma^*$)- and hadron production ($\gamma^*\phi p$)-planes for the $ep \rightarrow e'\phi p$ reaction defined in the laboratory (lab) and γ^*p center-of-mass (c.m.) frames, respectively.

where the Källén function is defined as $\lambda(x, y, z) \equiv x^2 + y^2 + z^2 - 2(xy + yz + zx)$.

We define some relevant variables as follows:

- $Q^2 = -k_1^2 > 0$, the negative four-momentum squared of the virtual photon, i.e., photon virtuality;
- $W^2 = (k_1 + p_1)^2 = M_N^2 + 2M_N\nu - Q^2$, the square of the invariant mass of the γ^*p system, where $\nu = E_e - E_{e'}$ is the energy transfer from the incident electron to the virtual photon in the laboratory (lab) frame;
- $t = (k_1 - k_2)^2$, the squared four-momentum transfer from the γ^* to the ϕ . $t' = |t - t_{min}|$, t_{min} being the minimal value of t at fixed Q^2 and W ;
- θ_e , the angle between the incident and scattered electrons;
- Φ , the angle between the electron scattering ($ee'\gamma^*$) and hadron production ($\gamma^*\phi p$) planes;
- θ_ϕ , the c.m. ϕ -meson angle relative to the virtual photon direction;

III. THEORETICAL FRAMEWORK

We employ an effective Lagrangian approach here. The production mechanisms under consideration are drawn with the relevant Feynman diagrams in Fig. 2, which includes Pomeron (\mathbb{P}) (a), Reggeized $f_1(1285)$ axial-vector (AV)-meson, (π, η) pseudoscalar (PS)-meson, and (a_0, f_0) scalar (S)-meson exchanges in the t channel (b), and direct ϕ -meson radiations via the proton in the s and u channels (c and d).

We can write the invariant amplitude as

$$\mathcal{M} = \varepsilon_\nu^*(\lambda) \bar{u}_{N'}(\lambda_f) \mathcal{M}^{\mu\nu} u_N(\lambda_i) \epsilon_\mu(\lambda_\gamma), \quad (4)$$

the helicities of the particles being given in parentheses. The forms of the invariant amplitudes are in complete analogy to the ϕ -meson photoproduction case [23] for the corresponding diagrams. The Dirac spinors of the incoming and outgoing nucleons are designated by u_N and $u_{N'}$, respectively. ϵ_μ and ε_ν denote the polarization vectors of the virtual photon and the ϕ meson, respectively. The extension of the photo- to electro-production of mesons entails an additional longitudinal component ($\lambda_\gamma = 0$) for the virtual-photon polarization vector in addition to the transverse ($\lambda_\gamma = \pm 1$) ones:

$$\epsilon(\pm 1) = \frac{1}{\sqrt{2}}(0, \mp 1, -i, 0), \quad \epsilon(0) = \frac{1}{\sqrt{Q^2}}(k, 0, 0, E_{\gamma^*}), \quad (5)$$

where $E_{\gamma^*} = \sqrt{k^2 - Q^2} = (M_N\nu - Q^2)/W$. The polarization vectors of the virtual photon and the ϕ meson satisfy the conventional completeness relations [22]

$$\sum_{\lambda_\gamma=0,\pm 1} (-1)^{\lambda_\gamma} \epsilon_\mu(\lambda_\gamma) \epsilon_\nu^*(\lambda_\gamma) = g_{\mu\nu} - \frac{k_{1\mu} k_{1\nu}}{k_1^2}, \quad \sum_{\lambda=0,\pm 1} \varepsilon_\mu(\lambda) \varepsilon_\nu^*(\lambda) = - \left[g_{\mu\nu} - \frac{k_{2\mu} k_{2\nu}}{M_\phi^2} \right]. \quad (6)$$

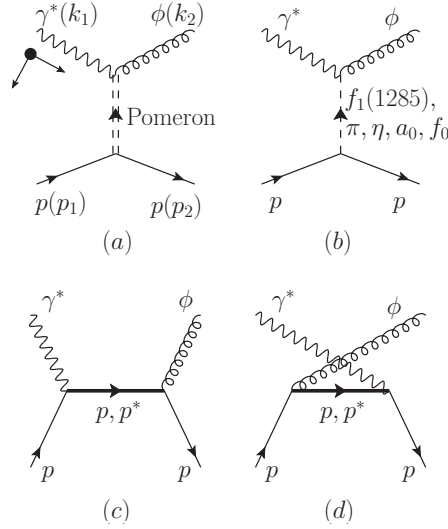


FIG. 2. Tree-level Feynman diagrams for $\gamma^* p \rightarrow \phi p$, which include Pomeron (a), Reggeized $f_1(1285)$ axial-vector-meson, (π, η) pseudoscalar-meson, and (a_0, f_0) scalar-meson exchanges in the t channel (b), and direct ϕ -meson radiations via the proton in the s and u channels (c and d).

A. Pomeron exchange

Figure 2(a) draws the Pomeron exchange that governs the scattering process in the high-energy and small t regions. We follow the Donnachie-Landshoff (DL) model [28] where a microscopic description of the Pomeron exchange in vector meson photo- and electroproduction is given in terms of nonperturbative Reggeized-two-gluon exchange based on the Pomeron-isoscalar-photon analogy (see Fig. 3) [29, 30].

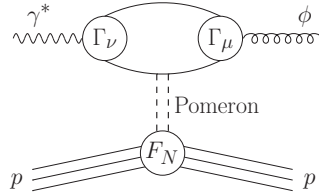


FIG. 3. Quark diagram for Pomeron exchange in the DL model, based on the Pomeron-isoscalar-photon analogy.

As a consequence, the invariant amplitude for the Pomeron exchange can be expressed as

$$\mathcal{M}_{\mathbb{P}}^{\mu\nu} = -M_{\mathbb{P}}(s, t) \left[\left(g^{\mu\nu} - \frac{k_2^\mu k_2^\nu}{k_2^2} \right) \not{k}_1 - \left(k_1^\nu - \frac{k_2^\nu k_1 \cdot k_2}{k_2^2} \right) \gamma^\mu - \left(\gamma^\nu - \frac{\not{k}_2 k_2^\nu}{k_2^2} \right) \not{k}_2 \right]. \quad (7)$$

One find that the last term in the square bracket on the r.h.s. breaks the gauge invariance and the following modification is performed to make it gauge invariant [31]:

$$k_2^\mu \rightarrow k_2^\mu - \frac{(p_1 + p_2)^\mu k_1 \cdot k_2}{(p_1 + p_2) \cdot k_1}. \quad (8)$$

Other prescriptions for the spin structure for conserving the gauge invariance are detailed in Ref. [32] but are not used in this work, because quantitative descriptions of ϕ -meson electroproduction with them are found to be very poor. The scalar function in Eq. (7) is given by

$$M_{\mathbb{P}}(s, t) = C_{\mathbb{P}} F_\phi(t) F_N(t) \frac{1}{s} \left(\frac{s}{s_{\mathbb{P}}} \right)^{\alpha_{\mathbb{P}}(t)} \exp \left[-\frac{i\pi}{2} \alpha_{\mathbb{P}}(t) \right]. \quad (9)$$

The strength factor is determined to be $C_{\mathbb{P}} = 3.6$ and the energy-scale factor to be $s_{\mathbb{P}} = (M_N + M_\phi)^2$. $F_N(t)$ and $F_\phi(t)$ stand for the nucleon isoscalar electromagnetic (EM) form factor [18, 33] and the form factor of the $\gamma \mathbb{P} \phi$

coupling [34, 35], respectively, and take the forms

$$F_N(t) = \frac{4M_N^2 - 2.8t}{(4M_N^2 - t)(1 - t/0.71)^2}, \quad F_\phi(t) = \frac{2\mu_0^2 \Lambda_\phi^2}{(Q^2 + \Lambda_\phi^2 - t)(2\mu_0^2 + Q^2 + \Lambda_\phi^2 - t)}, \quad (10)$$

The mass scale Λ_ϕ is proportional to the quark mass of the loop diagram in Fig. 3 and is chosen to be $\Lambda_\phi^2 = M_\phi^2$ as done previously. The momentum scale is given by $\mu_0^2 = 1.1 \text{ GeV}^2$ and the Pomeron trajectory is known to be $\alpha_{\mathbb{P}}(t) = 1.08 + 0.25t$.

B. $f_1(1285)$ axial-vector meson exchange

We first consider Reggeized $f_1(1285)$ AV-meson among meson exchanges depicted in Fig. 2(b). Its importance is indicated in elastic p - p scattering and elastic photoproduction of ρ - and ϕ -mesons due to its special relation to the axial anomaly through the matrix elements of the flavor singlet axial vector current [36] and is confirmed more specifically in ϕ -meson photoproduction done by the authors [23]. Thus we include $f_1(1285)$ AV-meson exchange in ϕ -meson electroproduction.

The effective Lagrangian for the AVV vertex is obtained from the hidden gauge approach [37]

$$\mathcal{L}_{\gamma\phi f_1} = g_{\gamma\phi f_1} \epsilon^{\mu\nu\alpha\beta} \partial_\mu A_\nu \partial^\lambda \partial_\lambda \phi_\alpha f_{1\beta}, \quad (11)$$

where f_1 denotes the $f_1(1285)$ field with its quantum number $I^G(J^{PC}) = 0^+(1^{++})$. The experimental data for the branching ratio (Br) $\text{Br}_{f_1 \rightarrow \phi\gamma} = 7.5 \times 10^{-4}$ and the decay width $\Gamma_{f_1} = 22.7 \text{ MeV}$ [38] lead to

$$g_{\gamma\phi f_1} = 0.17 \text{ GeV}^{-2}, \quad (12)$$

from Eq. (11).

The effective Lagrangian of the AV meson interaction with the nucleon takes the form

$$\mathcal{L}_{f_1 NN} = -g_{f_1 NN} \bar{N} \left[\gamma_\mu - i \frac{\kappa_{f_1 NN}}{2M_N} \gamma_\nu \gamma_\mu \partial^\nu \right] f_1^\mu \gamma_5 N. \quad (13)$$

The coupling constant $g_{f_1 NN}$ is obtained to be [39]

$$g_{f_1 NN} = 2.5 \pm 0.5, \quad (14)$$

and we use the maximum value $g_{f_1 NN} = 3.0$ in this work. Although the tensor term can have an effect on ϕ -meson electroproduction, we take the value of $\kappa_{f_1 NN}$ to be zero in this work for brevity.

The corresponding invariant amplitude reads

$$\mathcal{M}_{f_1}^{\mu\nu} = i \frac{M_\phi^2 g_{\gamma\phi f_1} g_{f_1 NN}}{t - M_{f_1}^2} \epsilon^{\mu\nu\alpha\beta} \left[-g_{\alpha\lambda} + \frac{q_{t\alpha} q_{t\lambda}}{M_{f_1}^2} \right] \left[\gamma^\lambda + \frac{\kappa_{f_1 NN}}{2M_N} \gamma^\sigma \gamma^\lambda q_{t\sigma} \right] \gamma_5 k_{1\beta}, \quad (15)$$

where $q_t = k_2 - k_1$. We substitute the exchange of the entire $f_1(1285)$ Regge trajectory for the above single $f_1(1285)$ meson exchange as [40]

$$P_{f_1}^{\text{Feyn}}(t) = \frac{1}{t - M_{f_1}^2} \rightarrow P_{f_1}^{\text{Regge}}(t) = \left(\frac{s}{s_{f_1}} \right)^{\alpha_{f_1}(t)-1} \frac{\pi \alpha'_{f_1}}{\sin[\pi \alpha_{f_1}(t)]} \frac{1}{\Gamma[\alpha_{f_1}(t)]} D_{f_1}(t), \quad (16)$$

such that the spin structures of the interaction vertices are kept and the Regge propagator effectively interpolates between small- and large-momentum transfers and can contribute to the high energy region properly. The Regge trajectory is determined to be $\alpha_{f_1}(t) = 0.99 + 0.028t$ [36] and the energy-scale factor $s_{f_1} = 1 \text{ GeV}^2$. The odd signature factor is given by [36]

$$D_{f_1}(t) = \frac{-1 + \exp(-i\pi \alpha_{f_1}(t))}{2}. \quad (17)$$

The invariant amplitude is modified by introducing the following form factors

$$g_{\gamma\phi f_1} \rightarrow g_{\gamma\phi f_1} F_{\gamma\phi f_1}(Q^2, t), \quad g_{f_1 NN} \rightarrow g_{f_1 NN} F_{f_1 NN}(t), \quad (18)$$

where

$$F_{\gamma\phi f_1}(t, Q^2) = \frac{\Lambda_{f_1}^2 - M_{f_1}^2}{\Lambda_{f_1}^2 - t} \frac{\Lambda_q^2}{\Lambda_q^2 + Q^2}, \quad F_{f_1 NN}(t) = \frac{\Lambda_{f_1}^2 - M_{f_1}^2}{\Lambda_{f_1}^2 - t}, \quad (19)$$

which are normalized at $t = M_{f_1}^2$ and $Q^2 = 0$ as $F_{\gamma\phi f_1}(t = M_{f_1}^2, Q^2 = 0) = F_{f_1 NN}$.

C. Pseudoscalar- and scalar-meson exchanges

Figure 2(b) also includes the contributions of the t -channel (π, η) PS- and (a_0, f_0) S-meson exchange diagrams. The EM interaction Lagrangians for the PS- and S-meson exchanges, respectively, can be written as

$$\begin{aligned}\mathcal{L}_{\gamma\Phi\phi} &= \frac{eg_{\gamma\Phi\phi}}{M_\phi} \epsilon^{\mu\nu\alpha\beta} \partial_\mu A_\nu \partial_\alpha \phi_\beta \Phi, \\ \mathcal{L}_{\gamma S\phi} &= \frac{eg_{\gamma S\phi}}{M_\phi} F^{\mu\nu} \phi_{\mu\nu},\end{aligned}\tag{20}$$

where $\Phi = \pi^0(135, 0^-)$, $\eta(548, 0^-)$ and $S = a_0(980, 0^+)$, $f_0(980, 0^+)$. The field-strength tensors for the photon and ϕ -meson are given by $F^{\mu\nu} = \partial^\mu A^\nu - \partial^\nu A^\mu$ and $\phi^{\mu\nu} = \partial^\mu \phi^\nu - \partial^\nu \phi^\mu$, respectively, and e the unit electric charge. The EM coupling constants are deduced from the $\phi \rightarrow \Phi\gamma$ and $\phi \rightarrow S\gamma$ decay widths

$$\Gamma_{\phi \rightarrow \Phi\gamma} = \frac{e^2}{12\pi} \frac{g_{\gamma\Phi\phi}^2}{M_\phi^2} \left(\frac{M_\phi^2 - M_\Phi^2}{2M_\phi} \right)^3, \quad \Gamma_{\phi \rightarrow S\gamma} = \frac{e^2}{3\pi} \frac{g_{\gamma S\phi}^2}{M_\phi^2} \left(\frac{M_\phi^2 - M_S^2}{2M_\phi} \right)^3.\tag{21}$$

With the ϕ -meson branching ratios of $\text{Br}_{\phi \rightarrow \pi\gamma} = 1.30 \times 10^{-3}$, $\text{Br}_{\phi \rightarrow \eta\gamma} = 1.303 \times 10^{-2}$, $\text{Br}_{\phi \rightarrow a_0\gamma} = 7.6 \times 10^{-5}$, and $\text{Br}_{\phi \rightarrow f_0\gamma} = 3.22 \times 10^{-4}$ and the value of $\Gamma_\phi = 4.249$ MeV [38], we obtain

$$g_{\gamma\pi\phi} = -0.14, \quad g_{\gamma\eta\phi} = -0.71, \quad g_{\gamma a_0\phi} = -0.77, \quad g_{\gamma f_0\phi} = -2.44.\tag{22}$$

The strong interaction Lagrangians for the PS- and S-meson exchanges read

$$\begin{aligned}\mathcal{L}_{\Phi NN} &= -ig_{\Phi NN} \bar{N} \Phi \gamma_5 N, \\ \mathcal{L}_{SNN} &= -g_{SNN} \bar{N} S N,\end{aligned}\tag{23}$$

respectively. We use the following strong coupling constants determined by the Nijmegen potential [41, 42]:

$$g_{\pi NN} = 13.0, \quad g_{\eta NN} = 6.34, \quad g_{a_0 NN} = 4.95, \quad g_{f_0 NN} = -0.51.\tag{24}$$

We obtain the invariant amplitudes for PS- and S-meson exchanges as

$$\begin{aligned}\mathcal{M}_\Phi^{\mu\nu} &= i \frac{e}{M_\phi} \frac{g_{\gamma\Phi\phi} g_{\Phi NN}}{t - M_\Phi^2} \epsilon^{\mu\nu\alpha\beta} k_{1\alpha} k_{2\beta} \gamma_5, \\ \mathcal{M}_S^{\mu\nu} &= \frac{e}{M_\phi} \frac{2g_{\gamma S\phi} g_{SNN}}{t - M_S^2 + i\Gamma_S M_S} (k_1 \cdot k_2 g^{\mu\nu} - k_1^\mu k_2^\nu),\end{aligned}\tag{25}$$

respectively, where we use $M_{a_0} = 980$ MeV, $M_{f_0} = 990$ MeV, and $\Gamma_{a_0, f_0} = 75$ MeV [38].

Here we also consider the form factors $F_{\gamma M\phi}(t, Q^2)$ and $F_{MNN}(t)$ for each vertex describing the dependence on the t and Q^2 similar to Eqs. (18) and (19):

$$F_{\gamma M\phi}(t, Q^2) = \frac{\Lambda_M^2 - M_M^2}{\Lambda_M^2 - t} \frac{\Lambda_q^2}{\Lambda_q^2 + Q^2}, \quad F_{MNN}(t) = \frac{\Lambda_M^2 - M_M^2}{\Lambda_M^2 - t},\tag{26}$$

where $M = (\Phi, S)$.

D. Direct ϕ -meson radiation term

It is argued that the direct ϕ -meson radiation term drawn in Figs. 2(c) and 2(d) gives a small contribution to the unpolarized cross sections but a very distinct contribution to some polarization observables in ϕ -meson photoproduction [23, 43]. Thus it is interesting to include this term in ϕ -meson electroproduction.

The effective Lagrangians for the direct ϕ -meson radiation contributions can be written as

$$\begin{aligned}\mathcal{L}_{\gamma NN} &= -e\bar{N} \left[\gamma_\mu - \frac{\kappa_N}{2M_N} \sigma_{\mu\nu} \partial^\nu \right] N A^\mu, \\ \mathcal{L}_{\phi NN} &= -g_{\phi NN} \bar{N} \left[\gamma_\mu - \frac{\kappa_{\phi NN}}{2M_N} \sigma_{\mu\nu} \partial^\nu \right] N \phi^\mu,\end{aligned}\tag{27}$$

where the anomalous magnetic moment of the proton is $\kappa_p = 1.79$ [38] and the vector and tensor coupling constants for the ϕ -meson to the nucleon are determined to be $g_{\phi NN} = -0.24$ and $\kappa_{\phi NN} = 0.2$ [44].

The ϕ -radiation invariant amplitudes are computed as

$$\begin{aligned}\mathcal{M}_{\phi \text{ rad}, s}^{\mu\nu} &= \frac{eg_{\phi NN}}{s - M_N^2} \left(\gamma^\nu - i \frac{\kappa_{\phi NN}}{2M_N} \sigma^{\nu\alpha} k_{2\alpha} \right) (\not{q}_s + M_N) \left(\gamma^\mu F_1^p + iF_2^p \frac{\kappa_N}{2M_N} \sigma^{\mu\beta} k_{1\beta} \right), \\ \mathcal{M}_{\phi \text{ rad}, u}^{\mu\nu} &= \frac{eg_{\phi NN}}{u - M_N^2} \left(\gamma^\mu F_1^p + iF_2^p \frac{\kappa_N}{2M_N} \sigma^{\mu\alpha} k_{1\alpha} \right) (\not{q}_u + M_N) \left(\gamma^\nu - i \frac{\kappa_{\phi NN}}{2M_N} \sigma^{\nu\beta} k_{2\beta} \right),\end{aligned}\quad (28)$$

for the s and u channels, respectively, with the EM form factors being involved. $q_{s,u}$ are the four momenta of the exchanged particles, i.e., $q_s = k_1 + p_1$ and $q_u = p_2 - k_1$.

Note that the Ward-Takahashi identity (WTI) is violated when a different form for the form factor F_1^p is used for the electric terms of the two invariant amplitudes. Thus we use the same form and can check the sum of them restores the WTI as

$$\begin{aligned}\mathcal{M}_{\phi \text{ rad}, s}^{\text{elec}}(\epsilon \rightarrow k_1) &= \frac{eg_{\phi NN}}{2k_1 \cdot p_1 - Q^2} \bar{u}_{N'} \left(\not{\epsilon}^* + \frac{\kappa_{\phi NN}}{4M_N} (\not{\epsilon}^* \not{k}_2 - \not{k}_2 \not{\epsilon}^*) \right) (2k_1 \cdot p_1 - Q^2) F_1^p u_N, \\ \mathcal{M}_{\phi \text{ rad}, u}^{\text{elec}}(\epsilon \rightarrow k_1) &= \frac{-eg_{\phi NN}}{2k_1 \cdot p_2 + Q^2} \bar{u}_{N'} F_1^p (2k_1 \cdot p_2 + Q^2) \left(\not{\epsilon}^* + \frac{\kappa_{\phi NN}}{4M_N} (\not{\epsilon}^* \not{k}_2 - \not{k}_2 \not{\epsilon}^*) \right) u_N,\end{aligned}\quad (29)$$

such that $\mathcal{M}_{\phi \text{ rad}}^{\text{elec}}(\epsilon \rightarrow k_1) \propto (F_1^p - F_1^p) = 0$. We follow the suggestion given by David and Workman [45] for the form factors:

$$\mathcal{M}_{\phi \text{ rad}} = (\mathcal{M}_{\phi \text{ rad}, s}^{\text{elec}} + \mathcal{M}_{\phi \text{ rad}, u}^{\text{elec}}) F_c(s, u)^2 F_1^p(Q^2) + \mathcal{M}_{\phi \text{ rad}, s}^{\text{mag}} F_N(s)^2 F_2^p(Q^2) + \mathcal{M}_{\phi \text{ rad}, u}^{\text{mag}} F_N(u)^2 F_2^p(Q^2). \quad (30)$$

Here a common form factor is introduced which conserves the on-shell condition and the crossing symmetry:

$$F_c(s, u) = 1 - [1 - F_N(s)][1 - F_N(u)], \quad (31)$$

with

$$F_N(x) = \frac{\Lambda_N^4}{\Lambda_N^4 + (x - M_N^2)^2}, \quad x = (s, u). \quad (32)$$

Since the magnetic terms are self-gauge-invariant, the form of Eq. (32) is just used for them.

Now, we give some details for the Dirac (F_1) and Pauli (F_2) form factors by using their relations with the Sachs one ($G_{E,M}$) [46]:

$$G_E(Q^2) = F_1(Q^2) - \kappa_N \tau F_2(Q^2), \quad G_M(Q^2) = \mu_N G_E(Q^2) = F_1(Q^2) + \kappa_N F_2(Q^2), \quad (33)$$

where $\tau = Q^2/4M_p^2$ and correspondingly,

$$F_1(Q^2) = \frac{G_E(Q^2) + \tau G_M(Q^2)}{1 + \tau}, \quad F_2(Q^2) = \frac{G_M(Q^2) - G_E(Q^2)}{\kappa_N(1 + \tau)}. \quad (34)$$

The Sachs form factors are parametrized for the proton and the neutron in the literature by

$$G_E^p(Q^2) \simeq G_D(Q^2), \quad G_M^p(Q^2) \simeq \mu_p G_D(Q^2), \quad G_E^n(Q^2) \simeq -\frac{a\mu_n\tau}{1+b\tau} G_D(Q^2), \quad G_M^n(Q^2) \simeq \mu_n G_D(Q^2), \quad (35)$$

with the dipole-type of form factor

$$G_D(Q^2) = \left[\frac{1}{1 + Q^2 \langle r^2 \rangle_E^p / 12} \right]^2, \quad (36)$$

where the electric root-mean-squared charge radius of the proton is given by $\langle r^2 \rangle_E^p = (0.863 \pm 0.004) \text{ fm}$ [47].

IV. NUMERICAL RESULTS AND DISCUSSIONS

We now discuss our numerical results from the present work. The remaining model parameters are the cutoff masses involved in the form factors. The cutoff masses for the t dependent form factors for meson exchanges are determined to be $\Lambda_{f_1, a_0, f_0} = 1.4$ and $\Lambda_{\pi, \eta} = 0.6$ GeV and that for the ϕ -meson radiations in Eq. (32) to be $\Lambda_N = 1.0$ GeV. We have shown that those phenomenological form factors provide a good description of ϕ -meson photoproduction at the considered energy region $W = (2-3)$ GeV and at even much higher one $W \lesssim 10$ GeV as well in our recent work [23]. The cutoff masses for the Q^2 dependent form factors for all meson exchanges are chosen to be $\Lambda_{Q^2} = 0.9$ GeV in common.

The cross section dependence on the angle Φ of meson electroproduction is decomposed into the transverse (T), longitudinal (L), and interference (TT, LT) parts as

$$\frac{d\sigma}{d\Phi} = \frac{1}{2\pi}(\sigma + \varepsilon\sigma_{\text{TT}} \cos 2\Phi + \sqrt{2\varepsilon(1+\varepsilon)}\sigma_{\text{LT}} \cos \Phi), \quad (37)$$

where $\sigma = \sigma_{\text{T}} + \varepsilon\sigma_{\text{L}}$. We refer to Appendix A for the explicit expressions for the T-L separated differential cross sections. If helicity is conserved in the s channel (SCHC), then the second and third terms vanish. The virtual-photon polarization parameter ε is defined by

$$\varepsilon = \left[1 + \frac{2k^2}{Q^2} \tan^2 \frac{\theta_e}{2} \right]^{-1}. \quad (38)$$

In all our calculations, we fix it to be $\varepsilon = 0.5$ because the available data to be used are carried out with the value close to it.

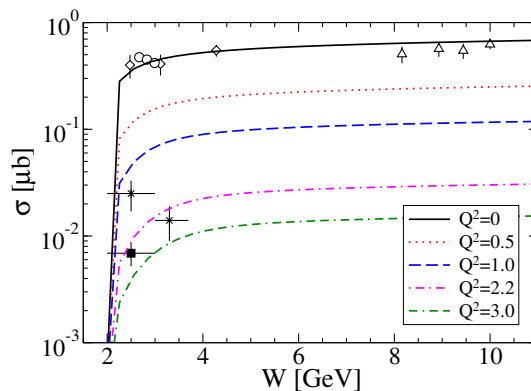


FIG. 4. Total cross sections for $\gamma^*p \rightarrow \phi p$ are plotted as a function of W for five different photon virtualities $Q^2 = (0, 0.5, 1.0, 2.2, 3.0)$ GeV². The ϕ photoproduction ($Q^2 = 0$) data are from Refs. [48] (diamond), [49] (circle), and [50] (triangle). The Cornell [8] (star) and CLAS [13] (square) data correspond to the results at $Q^2 = 2.2$ GeV².

Figure 4 displays the results of the total cross sections as a function of W for five different photon virtualities Q^2 . The slowly rising total cross sections with increasing W are kept for all values of Q^2 due to the dominant Pomeron contribution. The agreement with the experimental data [48–50] is good at the real photon limit $Q^2 = 0$ over the whole energy range. The magnitude of the total cross section when $Q^2 = 0.5$ GeV² reaches the level around 40% relative to that when $Q^2 = 0$. The results get more suppressed for higher values of Q^2 .

It is essential to investigate the separated components of the cross sections to clarify the different role of considered meson exchanges. The CLAS Collaboration [13] extracted the interference cross sections to be $\sigma_{\text{TT}} = -1.1 \pm 3.1$ nb and $\sigma_{\text{LT}} = 2.2 \pm 1.1$ nb from 6 bins of the $d\sigma/d\Phi$ data measured in the range of $W = (2.0-3.0)$ GeV and $Q^2 = (1.4-3.8)$ GeV² using the relation Eq. (37). The matrix element is extracted as well to be $r_{00}^{04} = 0.33 \pm 0.12$ from 5 bins of the polar angular distribution $W(\cos \theta_H)$. With the additional assumption of SCHC, the ratio of the longitudinal to transverse cross section is obtained to be $R = \sigma_{\text{L}}/\sigma_{\text{T}} = 1.05 \pm 0.38$. Also $r_{1-1}^1 = 0.38 \pm 0.23$ and $R = 0.72 \pm 0.3$ are obtained from 8 bins of the angular distribution $W(\psi = \phi_H - \Phi)$ under the SCHC approximation. Lastly, the longitudinal cross section is calculated to be $\sigma_{\text{L}}(Q^2 = 2.21 \text{ GeV}^2) = 4.5 \pm 1.1$ nb using the values of the average ratio $R = 0.85 \pm 0.24$ and of the average cross section $\sigma = 6.9 \pm 1.7$ nb [13]. The definitions of the matrix elements will be given later [51].

Figure 5 depicts the results of the transverse (σ_{T}) and longitudinal (σ_{L}) cross sections as functions of Q^2 in the upper and bottom panels, respectively, for three different c.m. energies W . We find that a predominant mechanism

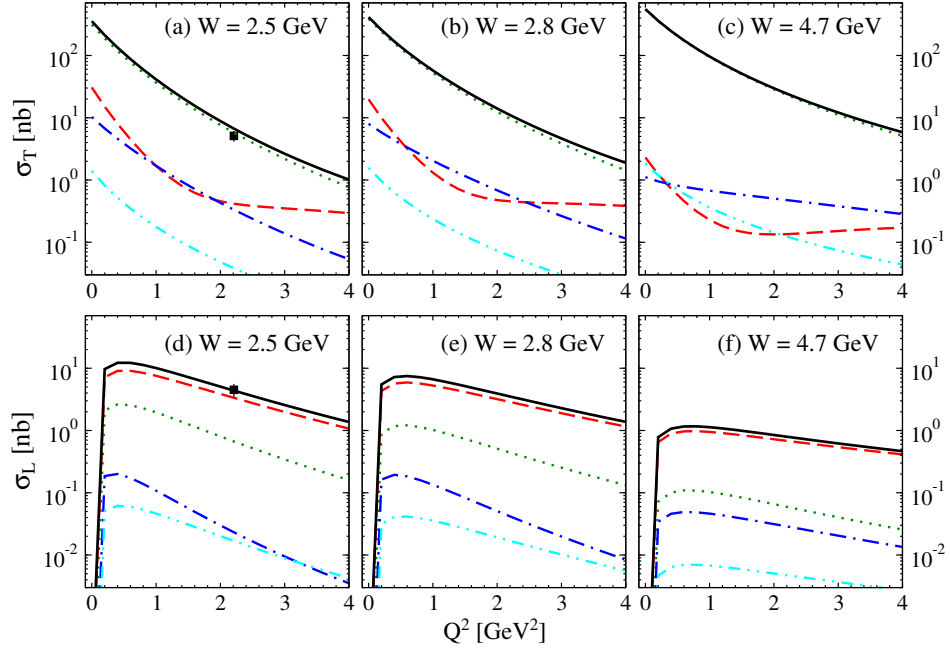


FIG. 5. Transverse σ_T (top panels) and longitudinal σ_L (bottom panels) cross sections are plotted as functions of Q^2 for three different c.m. energies labeled on each subplot. The green dotted, cyan dot-dot-dashed, blue dot-dashed, and red dashed curves stand for the contributions from the individual Pomeron, AV-meson, PS-meson, and S-meson exchanges, respectively. The black solid curves indicate the total contribution. The CLAS data in panels (a) and (d) are extracted from Ref. [13].

that contributes to the transverse cross section σ_T is the Pomeron exchange. The individual AV-, PS-, and S-meson exchanges all have little influences on σ_T for three $W = (2.5, 2.9, 4.7)$ GeV energy values. The contribution of the Pomeron exchange at $W = 2.5$ GeV and $Q^2 = 2.21$ GeV² is in very good agreement with the CLAS data as shown in Fig. 5(a). However, it is quite the opposite in the case of ρ -meson electroproduction. That is, the PS-meson exchange governs the transverse cross section σ_T due to the $M1$ spin transition $\gamma_T^* + \pi^0(\eta) \rightarrow \rho^0$ and Pomeron exchange is relatively much more suppressed at low c.m. energies ($W \sim$ a few GeV) and low photon virtualities ($Q^2 \sim$ a few GeV²) [22]. In this work, employing a strong form factor for the PS-meson exchange obviously overestimates the available ϕ -meson electroproduction CLAS data. Thus we use a rather small value of the cutoff mass as $\Lambda_{\pi,\eta} = 0.6$ GeV.

Meanwhile, the contribution of the Pomeron exchange alone for the longitudinal cross section σ_L is an order of magnitude smaller than that for σ_T at $W = 2.5$ GeV and $Q^2 = (1-4)$ GeV² as shown in Fig. 5(d). The difference becomes larger for higher c.m. energies $W = 2.5, 4.7$ GeV. The inclusion of S-meson exchange to the Pomeron exchange gives a sufficiently better description of σ_L due to the $E1$ spin transition $\gamma_L^* + a_0(f_0) \rightarrow \phi$. That is how the S-meson exchange form factor is determined, i.e., $\Lambda_{a_0,f_0} = 1.4$ GeV. As displayed in Fig. 5(d,e,f), the contribution of the S-meson exchange for σ_L is highly enhanced relative to σ_T and even prevails over that of the Pomeron exchange over all the ranges of W and Q^2 . All the amplitudes for the longitudinal photons must vanish at the limit $Q^2 = 0$ and this behavior is imposed explicitly in our calculation. For both σ_T and σ_L cases, the contribution of the AV-meson exchange is comparable to that of the PS-meson exchange or even more suppressed.

We present the results of the interference cross sections σ_{TT} and σ_{LT} in the upper and lower panels in Fig. 6, respectively. The overall results are the decrease of the absolute magnitudes with increasing W for all contributions, indicative of SCHC at relatively larger values of W and Q^2 . The meson-exchange contributions are all close to zero for σ_{TT} and the total contribution is entirely dependent on the Pomeron exchange which is the strongest at $Q^2 = 0$ and gradually decreases with increasing Q^2 . At $Q^2 \geq 2$ GeV², the results are consistent with zero for all values of W , which are within the CLAS data at $W = 2.5$ GeV and $Q^2 = 2.21$ GeV² as shown in Fig. 6(a).

Different patterns are observed for the results of the individual σ_{LT} cross sections in comparison to σ_{TT} as seen in Fig. 6(d,e,f). The overall positive sign applies to the Pomeron contribution for σ_{LT} . It is peaked at about 0.3 GeV² and falls off with increasing Q^2 . The signs of the PS- and S-meson contributions are the same each other but are opposite to that of the Pomeron contribution. The CLAS data shown in Fig. 6(d) is close to the Pomeron contribution. However, the inclusion of PS- and S-meson exchanges pulls down σ_{LT} and finally the total contribution reaches zero at $Q^2 = 2.21$ GeV². That is one more reason why PS-meson exchange should be suppressed in ϕ -meson

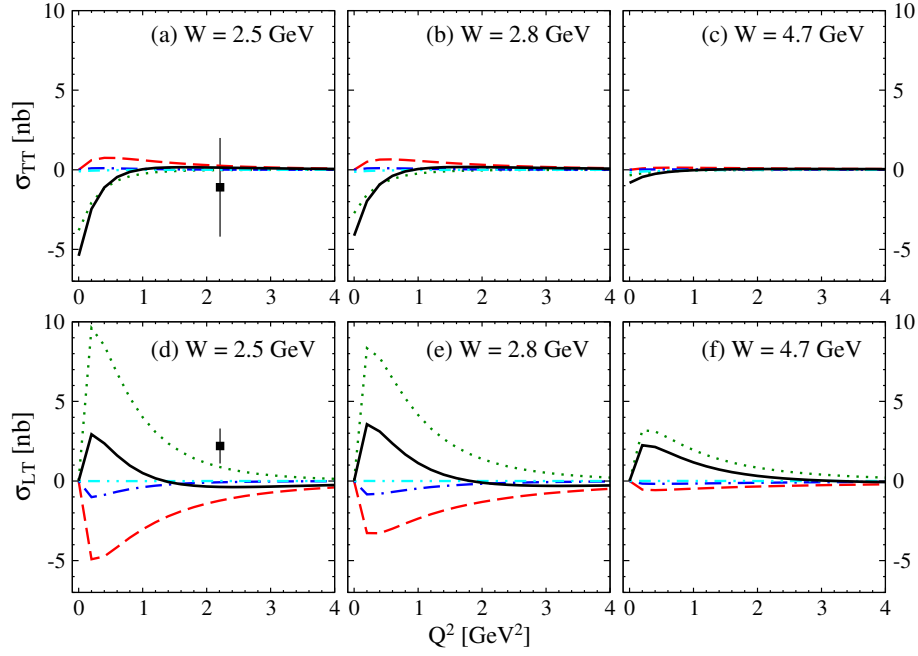


FIG. 6. The same as in Fig. 5 but for the interference cross sections σ_{TT} (upper panels) and σ_{LT} (bottom panels), respectively.

electroproduction. The small increase of the cutoff masses for both the PS- and S-meson form factors from the present ones makes the total results of σ_{LT} worse. The AV-meson exchange contributes almost negligibly to both σ_{TT} and σ_{LT} . However, note that its contribution to σ_{TT} is much more sensitive than that to σ_{LT} under the variation of the cutoff mass Λ_{f_1} .

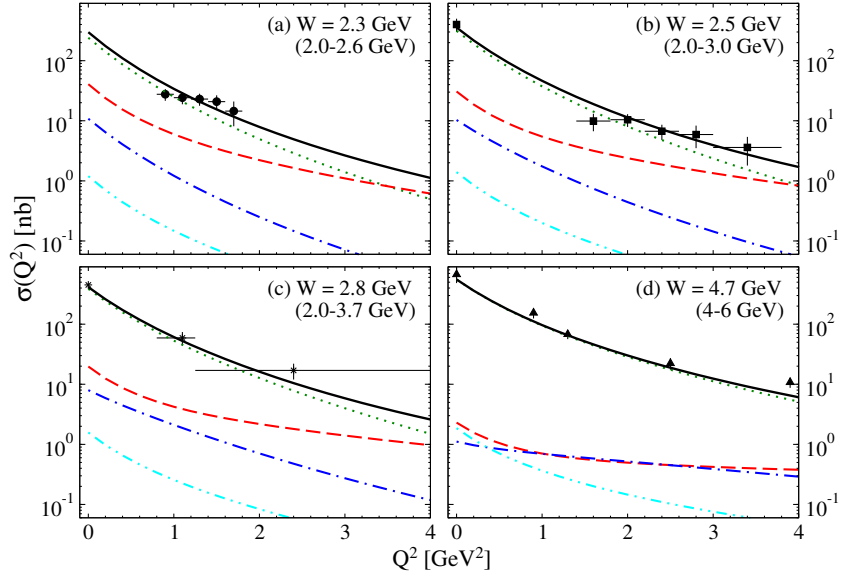


FIG. 7. Total cross sections are plotted as functions of Q^2 for four different c.m. energies labeled on each subplot. The curves are defined in the caption of Fig. 5. The circle [11] and square [13] data are from the CLAS Collaboration. The star and triangle data from the Cornell [8] and HERMES Collaboration [14], respectively. (b,c,d) The photoproduction points at $Q^2 = 0$ are from Refs. [48, 49].

Figure 7 depicts the results of the unpolarized total cross sections as functions of Q^2 for four different c.m. energies W . The model parameters are all constrained previously from the study of the separated cross sections although the available data on a Rosenbluth separation [52] are too poor to be a reliable basis for verifying the ϕ -meson electroproduction mechanism. It is interesting that the unpolarized cross sections are also well described over the whole

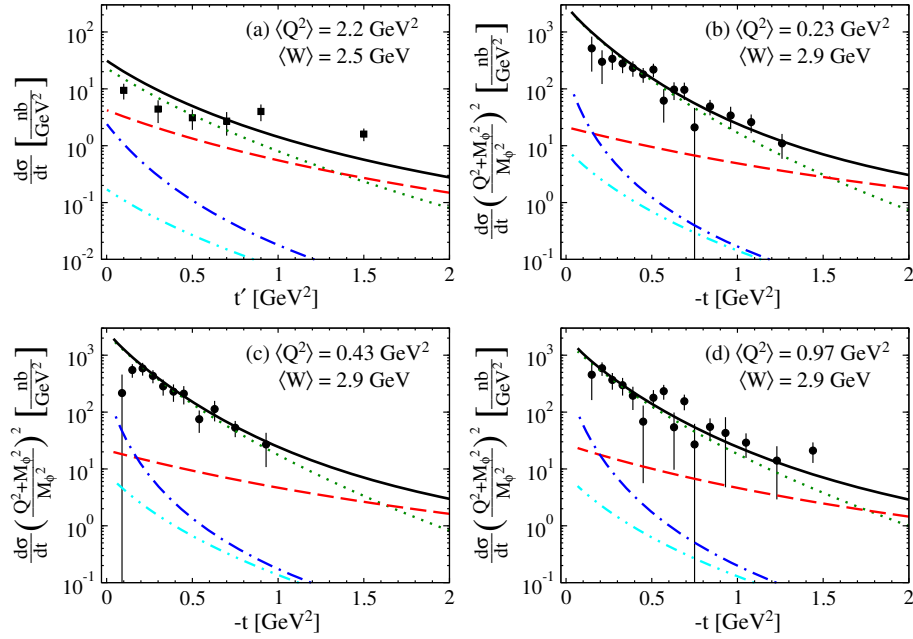


FIG. 8. (a) Differential cross section $d\sigma/dt$ is plotted as a function of $t' = |t - t_{\min}|$ and compared with the CLAS data [13]. (b,c,d) $d\sigma/dt$ multiplied by the factor $[(Q^2 + M_\phi^2)/M_\phi^2]^2$ is plotted as functions of $-t$ for three different photon virtualities labeled on each subplot at $W = 2.9$ GeV and compared with the Cornell data [6, 7]. The curves are defined in the caption of Fig. 5.

kinematical ranges of W and Q^2 , since the Pomeron exchange is mainly responsible for describing the experimental data. Although small, the effects of meson exchanges are revealed at larger values of Q^2 mostly due to the milder slope of the S-meson contribution than the Pomeron one. Our effective hadronic model accounts for the points at the real photon limit $Q^2 = 0$ as expected from Fig. 4,

The results of the differential cross section $d\sigma/dt$ are displayed in Fig. 8(a) at $Q^2 = 2.2$ GeV² and $W = 2.5$ GeV as a function of $t' \equiv |t - t_{\min}|$ where t_{\min} stands for the minimum value of t at fixed values Q^2 and W . Figure. 8(b,c,d) depict the results of $d\sigma/dt$, which are multiplied by the factor $[(Q^2 + M_\phi^2)/M_\phi^2]^2$ to eliminate the ϕ -propagator dependence, as functions of $-t$ for the three different photon virtualities Q^2 at $W = 2.9$ GeV. They corroborate our finding that the dominant contribution is the Pomeron exchange by which the t dependence is properly described. The strength of the S-meson exchange becomes larger than that of the Pomeron exchange at $|t| \gtrsim 1.5$ GeV². It should be mentioned that the a_0 - and π -meson contributions are more important than those of the f_0 and η mesons, respectively.

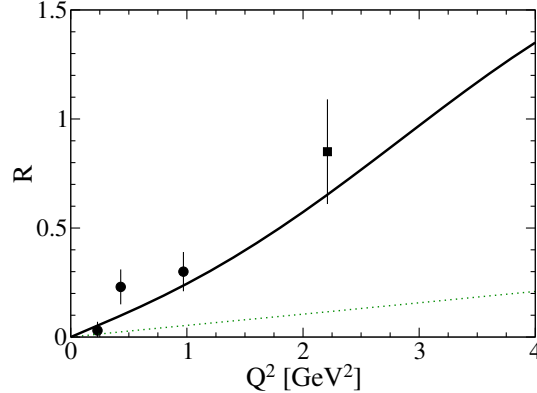


FIG. 9. The ratio of cross sections for longitudinally and transversely polarized photons $R = \sigma_L/\sigma_T$ is plotted as a function of Q^2 at $W = 2.5$ GeV. The green dotted and black solid curves stand for the Pomeron and total contributions, respectively. The data are from the Cornell [7] (circle) and CLAS Collaboration [13] (square).

We present the results of the ratio of the longitudinal to transverse cross section $R = \sigma_L/\sigma_T$ in Fig. 9 at $W = 2.5$ GeV

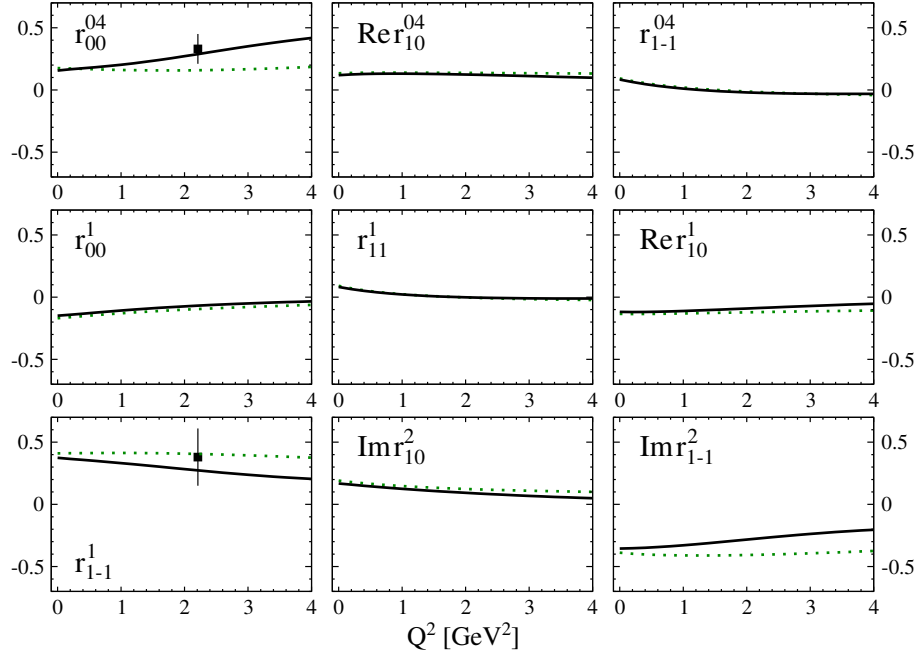


FIG. 10. Various matrix elements are plotted as functions of Q^2 at $W = 2.5$ GeV. The extracted data for r_{00}^{04} and r_{1-1}^1 are from the CLAS Collaboration [13].

although the Cornell data (circle) correspond to $W = 2.9$ GeV. Our results yield $R \leq 0.2$ for the Pomeron exchange, meaning that it mainly involves the transverse component in our given ranges of Q^2 . The agreement is noticeably better when the S-meson exchange is additionally included. Note that as the fixed c.m. energy W increases, the rise of R with respect to Q^2 becomes smaller as indicated in Fig. 5 where the transverse and longitudinal components of the Pomeron exchange exhibit the opposite pattern with W .

Finally, we make our predictions of various matrix elements, denoted by r_{ij}^α and related to the ϕ -meson spin-density matrix elements (SDMEs) [51]. When the experiments cannot conduct a σ_L/σ_T separation, r_{ij}^α can be represented as

$$\begin{aligned}
 r_{ij}^{04} &= \frac{\rho_{ij}^0 + \varepsilon R \rho_{ij}^4}{1 + \varepsilon R}, \\
 r_{ij}^\alpha &= \frac{\rho_{ij}^\alpha}{1 + \varepsilon R}, \quad \text{for } \alpha = (0-3), \\
 r_{ij}^\alpha &= \sqrt{R} \frac{\rho_{ij}^\alpha}{1 + \varepsilon R}, \quad \text{for } \alpha = (5-8).
 \end{aligned} \tag{39}$$

We refer to Appendix B for the definitions of the SDMEs ρ_{ij}^α . The matrix elements are described in the helicity frame, where the ϕ meson is at rest and its quantization axis is chosen to be antiparallel to the momentum of the outgoing proton in the c.m. frame of the hadron production process.

The results are shown in Fig. 10 as functions of Q^2 for nine different matrix elements labeled on each subplot. If SCHC holds, all presented matrix elements becomes zero except for r_{00}^{04} , r_{1-1}^1 , and $\text{Im} r_{1-1}^2$. It turns out that the SCHC approximation indeed applies at $Q^2 = (1-4)$ GeV². This conclusion is consistent with the results of Fig. 6 where SCHC is verified from the interference cross sections σ_{TT} and σ_{LT} . A good agreement with the CLAS data for r_{00}^{04} and r_{1-1}^1 is expected because they are extracted under the SCHC assumption.

It is useful to examine the relative contribution between the natural (N) and unnatural (U) parity exchange processes for the transverse cross section. The parity asymmetry is defined by [40]

$$P \equiv \frac{\sigma_T^N - \sigma_T^U}{\sigma_T^N + \sigma_T^U} = (1 + \varepsilon R)(2r_{1-1}^1 - r_{00}^1), \tag{40}$$

and our results yield $P \simeq 0.85$ and 0.95 for the Pomeron and total contributions, respectively. This observation indicates that the dominant mechanism of the transverse cross section is the natural-parity exchange. Also when a

purely natural-parity exchange is considered, e.g., the S-meson exchange, we have the following relation [12, 53]:

$$1 - r_{00}^{04} + 2r_{1-1}^{04} - 2r_{11}^1 - 2r_{1-1}^1 = 0. \quad (41)$$

For the Pomeron contribution, our results yield the values close to zero. The results from the total contribution yield $\simeq 0.1$ and thus the dominance of the natural-parity exchange is again verified.

V. SUMMARY

We have investigated the reaction mechanism of ϕ -meson electroproduction off the proton target based on the gauge-invariant effective Lagrangians in the tree-level Born approximation. Each contribution of the Pomeron, Reggeized $f_1(1285)$ AV-meson, (π, η) PS-meson, and (a_0, f_0) S-meson exchanges is scrutinized in the t channel diagram employing the CLAS and Cornell data. The direct ϕ -meson radiations via the proton are also taken into account in the s and u channels simultaneously to conserve gauge invariance. We summarize the essential points on which our model calculations have performed.

- The unpolarized cross sections σ show slow rising with increasing W . The results for the real photon limit $Q^2 = 0$ match with the available data very well. The magnitudes of σ become smaller with increasing Q^2 and the main contribution turns out to be Pomeron exchange. The cross sections σ give us no insight into what meson exchanges contributes to ϕ -meson electroproduction and thus it is necessary to examine the T-L separated cross sections.
- The Pomeron and S-meson exchanges dominate the transverse (σ_T) and longitudinal (σ_L) cross sections, respectively, at $Q^2 = (0-4)$ GeV² for three considered $W = 2.5, 2.9, 4.7$ GeV photon energies. Pomeron exchange alone is sufficient to describe the CLAS data on σ_T at $W = 2.5$ GeV and $Q^2 = 2.21$ GeV². Other meson contributions are more suppressed and the difference between the Pomeron and meson contributions becomes larger as W increases. Also the CLAS data on σ_L at the same W and Q^2 values are accounted for solely by the S-meson exchange. The Pomeron contribution for σ_T falls off faster than the S-meson contribution for σ_L as Q^2 increases.
- The interference cross sections σ_{TT} and σ_{LT} are found to be useful to clarify the role of AV- and PS-meson exchanges which is difficult from the study of σ_T and σ_L . First, for σ_{TT} , all meson-exchange contributions are compatible to zero and the total contribution is determined entirely by the Pomeron exchange which is negative in sign and the strongest at $Q^2 = 0$ and falls off steadily with increasing Q^2 . However, note that the AV-meson exchange is relatively more sensitive than other meson exchanges under the variation of each cutoff mass and its role can be more clearly verified when more experimental data on σ_{TT} are produced. Next, for the case of σ_{LT} , the patterns of each contribution are totally different from σ_{TT} . The Pomeron contribution is peaked at about $Q^2 = 0.3$ GeV² and falls off gradually with increasing Q^2 . The S-meson and PS-meson contributions also show similar peak positions. The signs of these two contributions are the same each other but are opposite to that of the Pomeron contribution. If the S-meson and PS-meson contributions increase from the present ones, then the total contribution will become negative and deviate from the CLAS data at $W = 2.5$ GeV and $Q^2 = 2.21$ GeV². Thus the S-meson and PS-meson contributions must be small from the present results. The effect of the AV-meson exchange is almost negligible. For both σ_{TT} and σ_{LT} cases, the total contribution is close to zero at $Q^2 = (1-4)$ GeV², indicating SCHC.
- The t dependence of the differential cross sections $d\sigma/dt$ is also well described in the range of $|t| = (0-2)$ GeV². The Pomeron exchange dominates over the whole t regions. Although small, the role of the meson exchanges are significant only at $|t| \gtrsim 1$ GeV² mostly from the S-meson exchange. The ratio of the longitudinal to transverse cross section $R = \sigma_L/\sigma_T$ rises linearly with increasing Q^2 . R for the total contribution is about 7 times larger than that for the Pomeron contribution due to the S-meson contribution and is good agreement with the experimental data.
- We examine various matrix elements defined in helicity frame which is in favor of SCHC. We find that the values of $\text{Re } r_{10}^{04}, r_{1-1}^{04}, r_{00}^1, r_{11}^1, \text{Re } r_{10}^1$, and $\text{Im } r_{10}^2$ are close to zero at $Q^2 = (1-4)$ GeV² and thus SCHC holds. Our results match with the CLAS data on r_{00}^{04} and r_{1-1}^1 . When we come to ρ -meson electroproduction, in the similar low Q^2 and W ranges, it is difficult to draw a firm conclusion concerning SCHC although most physical observables seem to support SCHC [10]. On the contrary, SCHC is known to be broken in w -meson electroproduction because of the different contributions of Pomeron and various meson exchanges [12]. Also a small but significant violation of SCHC is found in ϕ -meson electroproduction in the high ranges of Q^2 and W [4], where the generalized parton distributions (GPD) and factorization of scales will become relevant.

- The parity asymmetry provides us with the information of the relative strength of the natural to unnatural parity exchanges in the t channel for σ_T . Our results yield $P \simeq 0.95$, implying that the transverse cross section is mainly governed by the natural-parity exchange. Meanwhile, the contribution of the direct ϕ -meson radiations via the proton is found to be almost negligible.

The currently available data on ϕ -meson electroproduction are very limited and new experiments at current or future electron facilities are strongly called for. We can gain a deeper understanding of ϕ -meson electroproduction mechanism by comparing our numerical results with those of the GPD-based model. It is valuable to extend the present work to electroproductions of ρ -, ω -, and J/ψ -mesons. The corresponding work is underway.

ACKNOWLEDGMENTS

The authors are grateful to A. Hosaka (RCNP) for fruitful discussions. This work is supported in part by the National Research Foundation of Korea (NRF) funded by the Ministry of Education, Science and Technology (MSIT) (NRF-2018R1A5A1025563). The work of S.H.K. was supported by NRF-2019R1C1C1005790. The work of S.i.N. was also supported partly by NRF-2019R1A2C1005697.

Appendix A: APPENDIX A: T-L SEPARATED DIFFERENTIAL CROSS SECTIONS

The separated components of the differential cross sections in the Rosenbluth formula [52] take the forms

$$\begin{aligned}
\frac{1}{\mathcal{N}} \frac{d\sigma_T}{dt} &= \frac{1}{2} \sum_{\lambda_\gamma=\pm 1} |\overline{\mathcal{M}^{(\lambda_\gamma)}}|^2, \\
\frac{1}{\mathcal{N}} \frac{d\sigma_L}{dt} &= |\overline{\mathcal{M}^{(\lambda_\gamma=0)}}|^2, \\
\frac{1}{\mathcal{N}} \frac{d\sigma_{TT}}{dt} &= -\frac{1}{2} \sum_{\lambda_\gamma=\pm 1} \overline{\mathcal{M}^{(\lambda_\gamma)}} \mathcal{M}^{(-\lambda_\gamma)*}, \\
\frac{1}{\mathcal{N}} \frac{d\sigma_{LT}}{dt} &= -\frac{1}{2\sqrt{2}} \sum_{\lambda_\gamma=\pm 1} \lambda_\gamma (\overline{\mathcal{M}^{(0)}} \mathcal{M}^{(\lambda_\gamma)*} + \overline{\mathcal{M}^{(\lambda_\gamma)}} \mathcal{M}^{(0)*}),
\end{aligned} \tag{A1}$$

for vector-meson electroproduction. The common kinematical factor \mathcal{N} is defined by

$$\mathcal{N} = [32\pi(W^2 - M_N^2)Wk]^{-1}. \tag{A2}$$

Here the squared invariant amplitude is expressed as

$$|\overline{\mathcal{M}^{(\lambda_\gamma)}}|^2 = \frac{1}{2} \sum_{\lambda_i, \lambda_f, \lambda} \mathcal{M}_{\lambda_f \lambda; \lambda_i \lambda_\gamma} \mathcal{M}_{\lambda_f \lambda; \lambda_i \lambda_\gamma}^*, \tag{A3}$$

where the averaging over the incoming nucleon (λ_i) helicity and the summation over the outgoing ϕ meson (λ) and nucleon (λ_f) helicities are indicated. $\mathcal{M}_{\lambda_f \lambda_V; \lambda_i \lambda_\gamma}^*$ stands for the complex conjugate of the amplitude $\mathcal{M}_{\lambda_f \lambda_V; \lambda_i \lambda_\gamma}$. Note that the differential cross sections have the following relations:

$$\frac{d\Omega_\phi}{dt} = \frac{\pi}{|\mathbf{k}||\mathbf{p}|}. \tag{A4}$$

Appendix B: APPENDIX B: SPIN-DENSITY MATRIX ELEMENTS

We obtain nine components of the spin-density matrix elements (SDMEs) of the ϕ meson if those of the virtual photon are decomposed into the standard set of nine matrices Σ^α ($\alpha = 0 - 8$) [51]:

$$\rho_{\lambda\lambda'}^\alpha = \frac{1}{2N_\alpha} \sum_{\lambda_\gamma, \lambda'_\gamma, \lambda_i, \lambda_f} \mathcal{M}_{\lambda_f \lambda; \lambda_i \lambda_\gamma} \Sigma_{\lambda_\gamma \lambda'_\gamma}^\alpha \mathcal{M}_{\lambda_f \lambda'; \lambda_i \lambda'_\gamma}^*, \tag{B1}$$

where the normalization factors N_α are defined by

$$\begin{aligned} N_\alpha &= N_T = \frac{1}{2} \sum_{\lambda_\gamma=\pm 1, \lambda, \lambda_i, \lambda_f} |\mathcal{M}_{\lambda_f \lambda; \lambda_i \lambda_\gamma}|^2 \quad \text{for } \alpha = (0-3), \\ N_\alpha &= N_L = \sum_{\lambda, \lambda_i, \lambda_f} |\mathcal{M}_{\lambda_f \lambda; \lambda_i 0}|^2, \quad \text{for } \alpha = 4, \\ N_\alpha &= \sqrt{N_M N_L} \quad \text{for } \alpha = (5-8). \end{aligned} \tag{B2}$$

We finally obtain the SDMEs in terms of the helicity amplitudes:

$$\begin{aligned} \rho_{\lambda\lambda'}^0 &= \frac{1}{2N_T} \sum_{\lambda_\gamma=\pm 1} \mathcal{M}_{\lambda\lambda_\gamma} \mathcal{M}_{\lambda'\lambda_\gamma}^*, \\ \rho_{\lambda\lambda'}^1 &= \frac{1}{2N_T} \sum_{\lambda_\gamma=\pm 1} \mathcal{M}_{\lambda-\lambda_\gamma} \mathcal{M}_{\lambda'\lambda_\gamma}^*, \\ \rho_{\lambda\lambda'}^2 &= \frac{i}{2N_T} \sum_{\lambda_\gamma=\pm 1} \lambda_\gamma \mathcal{M}_{\lambda-\lambda_\gamma} \mathcal{M}_{\lambda'\lambda_\gamma}^*, \\ \rho_{\lambda\lambda'}^3 &= \frac{1}{2N_T} \sum_{\lambda_\gamma=\pm 1} \lambda_\gamma \mathcal{M}_{\lambda\lambda_\gamma} \mathcal{M}_{\lambda'\lambda_\gamma}^*, \\ \rho_{\lambda\lambda'}^4 &= \frac{1}{N_L} \mathcal{M}_{\lambda 0} \mathcal{M}_{\lambda' 0}^*, \\ \rho_{\lambda\lambda'}^5 &= \frac{1}{\sqrt{2N_T N_L}} \sum_{\lambda_\gamma=\pm 1} \frac{\lambda_\gamma}{2} (\mathcal{M}_{\lambda 0} \mathcal{M}_{\lambda'\lambda_\gamma}^* + \mathcal{M}_{\lambda\lambda_\gamma} \mathcal{M}_{\lambda' 0}^*), \\ \rho_{\lambda\lambda'}^6 &= \frac{i}{\sqrt{2N_T N_L}} \sum_{\lambda_\gamma=\pm 1} \frac{1}{2} (\mathcal{M}_{\lambda 0} \mathcal{M}_{\lambda'\lambda_\gamma}^* - \mathcal{M}_{\lambda\lambda_\gamma} \mathcal{M}_{\lambda' 0}^*), \\ \rho_{\lambda\lambda'}^7 &= \frac{1}{\sqrt{2N_T N_L}} \sum_{\lambda_\gamma=\pm 1} \frac{1}{2} (\mathcal{M}_{\lambda 0} \mathcal{M}_{\lambda'\lambda_\gamma}^* + \mathcal{M}_{\lambda\lambda_\gamma} \mathcal{M}_{\lambda' 0}^*), \\ \rho_{\lambda\lambda'}^8 &= \frac{i}{\sqrt{2N_T N_L}} \sum_{\lambda_\gamma=\pm 1} \frac{\lambda_\gamma}{2} (\mathcal{M}_{\lambda 0} \mathcal{M}_{\lambda'\lambda_\gamma}^* - \mathcal{M}_{\lambda\lambda_\gamma} \mathcal{M}_{\lambda' 0}^*), \end{aligned} \tag{B3}$$

where the summation over the incoming and outgoing nucleon helicities are omitted, for brevity, i.e.,

$$\sum_{\lambda_i, \lambda_f} \mathcal{M}_{\lambda_f \lambda; \lambda_i \lambda_\gamma} \mathcal{M}_{\lambda_f \lambda'; \lambda_i \lambda_\gamma}^* = \mathcal{M}_{\lambda\lambda_\gamma} \mathcal{M}_{\lambda'\lambda_\gamma}^*. \tag{B4}$$

We have the following relations:

$$\begin{aligned} \rho_{\lambda\lambda'}^\alpha &= (-1)^{\lambda-\lambda'} \rho_{-\lambda-\lambda'}^\alpha, \quad (\alpha = 0, 1, 4, 5, 8), \\ \rho_{\lambda\lambda'}^\alpha &= -(-1)^{\lambda-\lambda'} \rho_{-\lambda-\lambda'}^\alpha, \quad (\alpha = 2, 3, 6, 7). \end{aligned} \tag{B5}$$

-
- [1] J. Breitweg *et al.* (ZEUS Collaboration), Eur. Phys. J. C **6**, 603 (1999).
 - [2] F. D. Aaron *et al.* (H1 Collaboration), JHEP **1005**, 032 (2010).
 - [3] J. Breitweg *et al.* (ZEUS Collaboration), Phys. Lett. B **487**, 273 (2000).
 - [4] C. Adloff *et al.* (H1 Collaboration), Phys. Lett. B **483**, 360 (2000).
 - [5] S. Chekanov *et al.* (ZEUS Collaboration), Nucl. Phys. **B718**, 3 (2005).
 - [6] R. L. Dixon *et al.*, Phys. Rev. Lett. **39**, 516 (1977).
 - [7] R. L. Dixon *et al.*, Phys. Rev. D **19**, 3185 (1979).
 - [8] D. G. Cassel *et al.*, Phys. Rev. D **24**, 2787 (1981).
 - [9] C. Hadjidakis *et al.* (CLAS Collaboration), Phys. Lett. B **605**, 256 (2005).

- [10] S. A. Morrow *et al.* (CLAS Collaboration), Eur. Phys. J. A **39**, 5 (2009).
- [11] K. Lukashin *et al.* (CLAS Collaboration), Phys. Rev. C **63**, 065205 (2001); **64**, 059901 (E) (2001).
- [12] L. Morand *et al.* (CLAS Collaboration), Eur. Phys. J. A **24**, 445 (2005).
- [13] J. P. Santoro *et al.* (CLAS Collaboration), Phys. Rev. C **78**, 025210 (2008).
- [14] A. Borissov (HERMES Collaboration), Acta Phys. Polon. B **31**, 2353 (2000).
- [15] A. Airapetian *et al.* (HERMES Collaboration), Eur. Phys. J. C **71**, 1609 (2011).
- [16] A. Airapetian *et al.* (HERMES Collaboration), Eur. Phys. J. C **74**, 3110 (2014); **76**, 162 (E) (2016).
- [17] A. Airapetian *et al.* (HERMES Collaboration), Eur. Phys. J. C **77**, 378 (2017).
- [18] J. M. Laget and R. Mendez-Galain, Nucl. Phys. **A581**, 397 (1995).
- [19] J. M. Laget, Phys. Lett. B **489**, 313 (2000).
- [20] J. M. Laget, Nucl. Phys. A **699**, 184 (2002).
- [21] J. M. Laget, Phys. Rev. D **70**, 054023 (2004).
- [22] I. T. Obukhovskiy *et al.*, Phys. Rev. D **81**, 013007 (2010).
- [23] S. H. Kim and S. i. Nam, Phys. Rev. C **100**, 065208 (2019).
- [24] H. Seraydaryan *et al.* (CLAS Collaboration), Phys. Rev. C **89**, 055206 (2014).
- [25] B. Dey *et al.* (CLAS Collaboration), Phys. Rev. C **89**, 055208 (2014); **90**, 019901 (A) (2014).
- [26] Y. s. Oh and T. S. H. Lee, Phys. Rev. C **69**, 025201 (2004).
- [27] N. C. Wei, F. Huang, K. Nakayama, and D. M. Li, Phys. Rev. D **100**, 114026 (2019).
- [28] A. Donnachie and P. V. Landshoff, Nucl. Phys. **B244**, 322 (1984); **B267**, 690 (1986); Phys. Lett. B **185**, 403 (1987).
- [29] M. A. Pichowsky and T. S. H. Lee, Phys. Lett. B **379**, 1 (1996).
- [30] M. A. Pichowsky and T. S. H. Lee, Phys. Rev. D **56**, 1644 (1997).
- [31] A. I. Titov and T. S. H. Lee, Phys. Rev. C **67**, 065205 (2003).
- [32] A. I. Titov, Y. Oh, S. N. Yang, and T. Morii, Phys. Rev. C **58**, 2429 (1998).
- [33] A. Donnachie and P. V. Landshoff, Nucl. Phys. **B311**, 509 (1989).
- [34] G. A. Jaroszkiewicz and P. V. Landshoff, Phys. Rev. D **10**, 170 (1974).
- [35] A. Donnachie and P. V. Landshoff, Nucl. Phys. **B231**, 189 (1984).
- [36] N. I. Kochelev, D. P. Min, Y. Oh, V. Vento, and A. V. Vinnikov, Phys. Rev. D **61**, 094008 (2000).
- [37] N. Kaiser and U. G. Meissner, Nucl. Phys. **A519**, 671 (1990).
- [38] M. Tanabashi *et al.* (Particle Data Group), Phys. Rev. D **98**, 030001 (2018).
- [39] M. Birkel and H. Fritzsche, Phys. Rev. D **53**, 6195 (1996).
- [40] A. Donnachie *et al.*, *Pomeron Physics and QCD* (Cambridge University Press, Cambridge, England, 2002).
- [41] V. G. J. Stoks and Th. A. Rijken, Phys. Rev. C **59**, 3009 (1999).
- [42] T. A. Rijken, V. G. J. Stoks and Y. Yamamoto, Phys. Rev. C **59**, 21 (1999).
- [43] A. I. Titov, T.-S. H. Lee, H. Toki, and O. Streltsova, Phys. Rev. C **60**, 035205 (1999).
- [44] U. G. Meissner, V. Mull, J. Speth, and J. W. van Orden, Phys. Lett. B **408**, 381 (1997).
- [45] R. M. Davidson and R. Workman, Phys. Rev. C **63**, 025210 (2001).
- [46] S. i. Nam, Phys. Rev. D **96**, 076021 (2017).
- [47] J. J. Kelly, Phys. Rev. C **70**, 068202 (2004).
- [48] J. Ballam *et al.*, Phys. Rev. D **7**, 3150 (1973).
- [49] D. P. Barber *et al.*, Z. Phys. C **12**, 1 (1982).
- [50] R. M. Egloff *et al.*, Phys. Rev. Lett. **43**, 657 (1979).
- [51] K. Schilling and G. Wolf, Nucl. Phys. **B61**, 381 (1973).
- [52] M. N. Rosenbluth, Phys. Rev. **79**, 615 (1950).
- [53] M. Tytgat, DESY-THESIS-2001-018 (2001).